CATTLE PRACTICE ISSN 0969-1251
2025 33(3)

DOI Link: https://doi.org/10.59671/Vfn6R
Vol.33, Issue.3, Part.1, March 2025, PP.2-22

Removal of Indigo Carmine Dye Using NiO Nanoparticles Extracted from *Citrus Limon* Leaf Extract.

[a]Fatima A. S. Al-Yusufy* [b]Tasneem I. Hussein, [c]Zulfa M. Abaker, [d]Fatima A. Al-Qadri, [e]Bakheit Mustafa, [f]Mukhtar Ismail, [g]H. A. Asmaly.

[a,b,c,e,f] Department of Chemistry, College of Science, Qassim University, Buraydah, 51452, Saudi Arabia.
[d] Department of Chemistry, Faculty of Science and Arts at Sharurah, Najran University, Saudi Arabia.
[g] Interdisciplinary Research Center for Hydrogen and Carbon Management (IRC-HTCM),
Research Institute, King Fahd University of Petroleum and Minerals (KFUPM), Saudi Arabia.
* Corresponding Author's email:f.yousefi@qu.edu.sa

Received Jan 2025 Accepted Feb 2025 Published March 2025

Abstract

In the current study a green approach was carried out to prepare nickel oxide nanoparticles (NiO-NPs) using *Citrus limon* leaf extract and nickel nitrate hexahydrate $Ni(NO_3)_2 \bullet 6H_2O$ as a precursor. The synthesized NiO-NPs were characterized using the Fourier transform infrared spectroscopy (FTIR), x-ray diffraction (XRD). The FTIR spectrum showed a strong broad band at 422 cm^{-1} corresponding to Ni–O stretching vibration of the NiO nanocrystals. The XRD pattern revealed that NiO-NPs possess a cubic crystalline structure with an average crystallite size of 14.5 nm. The NiO-NPs were employed as an adsorbent for the removal of Indigo Carmine (IC) dye from aqueous solutions under different functional parameters, including adsorbent weight, adsorption duration, temperature, pH value, and initial IC dye concentration. The adsorption processes were monitored using UV-vis. spectrophotometry. The results obtained showed that the Langmuir model of adsorption isotherm analysis fits the equilibrium experimental data more accurately than the Freundlich model, and the pseudo-second order (PSO) kinetic model was more appropriate than the pseudo-first order (PFO) kinetic model. The thermodynamic estimation of the adsorption of IC onto NiO-NPs revealed a spontaneous exothermic process with an increase in randomness, with negative Gibbs free energy (ΔG^o) and enthalpy (ΔH^o) values and a positive entropy (ΔS^o) value.

Keywords: Green Synthesis, *Citrus limon* leaf extract, NiO nanoparticles, dye-removal, Adsorption parameters.

1. Introduction

The development of cost-effective and ecologically friendly technology for the removal of dyes from contaminated effluents is critical to reducing the environmental impact of dyes and textile wastewaters. IC dye is widely used in the textile industry because of its color intensity. It is categorized as a poisonous dye since it causes harm to human health when it comes into contact with the skin and eyes (1, 2).

Many conventional techniques have been modified to remediate effluents contaminated with organic dyes. These technologies, however, are inefficient and have a number of drawbacks, resulting in significant operational expenses. Thus, establishing low-cost technology for effective removal of IC from contaminated effluents is challenging (3, 4). Adsorption seems to be an efficient, reliable, and very promising technique for dye removal due to its simplicity and effectiveness. A wide range of nanomaterials have been created and used as adsorbents for wastewater treatment (1, 5-7). Consequently, they are cost-effective and have remarkable characteristics such as small size, high surface area, high adsorption capacity, availability of numerous reactive sites, and high regeneration capacity. Amongst the metal oxides employed, NiO-NPs possess unique features that make them ideal for various applications, including photocatalytic degradation of organic dyes, and wastewater pollution removal (3, 5, 6). With a polar surface, NiO-NPs could offer some benefits in the adsorption of certain pollutants. The environmental benefits of NiO-NPs in the adsorption of inorganic pollutants and toxic dyes are critical to ensuring a clean environment (6, 7).

Citrus limon, a native species of tropical and subtropical Southeast Asia and North India, belongs to the plant family *Rutaceae.* It is a flowering tree with evergreen leaves that can grow up to 6 m tall and has thick spines. The leaves are oval, dark, leathery, and green. *Citrus limon* is a yellow or green edible fruit most commonly known as lemon. Previous phytochemical studies (8-10) conducted on this plant revealed that the *citrus limon* leaves are rich in various bioactive compounds such as flavonoids, phenols, alkaloids, and saponins. Such functional groups act as a capping moiety to NiO NPs, stabilizing them and preventing agglomeration. An alternative to the chemical and physical methods, the green synthesis is featured as an eco-friendly and cost-effective approach (5, 11). The synthesis of NiO-NPs was carried out using $Ni(NO_3)_2 \bullet 6H_2O$ in aqueous citrus limon leaf extract as a reducing agent and capping/stabilizer to control the particle size during NiO-NPs synthesis. The biosynthesized nanoparticles were characterized using FTIR, XRD, scanning electron microscopy (SEM), and Brunauer-Emmett-Teller (BET). Furthermore, for better understanding of the adsorption process, the adsorption isotherms and the adsorption kinetics using the most used models were estimated.

This study aims to i) prepare NiO-NPs via a green approach using *citrus limon* leaf extract as a reducing and stabilizing agent. ii) Examine the adsorbent capacity of

the biosynthesized nanoparticles in removing indigo carmine dye from aqueous solutions under different adsorption parameters: contact time, pH, sorbent dosage, dye initial concentration, and temperature. iii) Investigate the isotherm, kinetic, and thermodynamic parameters exploited from the batch adsorption results using well-known theoretical models.

2. Materials and Methods

Chemicals and Reagents

All the chemicals purchased were of analytical reagent grade. $Ni(NO_3)_2 \bullet 6H_2O$, (BDH chemicals, Middle East LLC, UAE 98%), sodium hydroxide (NaOH, Fluka Honeywell, Seelze, Germany, 99.9%), HCl (Fluka Honeywell, Seelze, Germany, 37%), ethanol (Sigma-Aldrich, Milwaukee, United States), and indigo carmine (IC, Merk, Damstadt, Germany). All aqueous solutions were prepared using double distilled water. HCl, NaOH, and buffers were utilized to adjust the pH of the working solutions.

Preparation and Phytochemical analysis of the *citrus limon* leaf extract

The preparation method of the leaf extract was adapted from Hooda et al. (12). *Citrus limon* leaves were collected from a private house garden in Ar Rass city, Qassim, Saudi Arabia. The fresh leaves were washed using running tap water, followed by distilled water to remove dust particles, then dried in dark at ambient temperature for 24 h. The dry leaves were then powdered using an electric grinder. 20 g of the leaf powder was transferred to an Erlenmeyer flask containing 400 mL of distilled water. The mixture was stirred at 80°C with a magnetic stirrer at 900 rpm for 1 h. Subsequently, after cooling to ambient temperature, the mixture was filtered using a Buchner funnel through Whatman no. 1 filter paper. Finally, the filtrate was kept at 4°C for further use. The phytochemical analysis according to previous studies (13, 14) were carried out to test for the presence of phytochemical constituents, namely, flavonoids, alkaloids, phenols and saponins.

Test for flavonoids: A volume of 1 ml leaf extract was treated with 1 mL of NaOH.

Test for alkaloids: A volume of 1 ml leaf extract was acidified by adding 1 mL of 1.5% v/v HCl solution, and then 1 mL of Wagner's reagent was added.

Test for phenols: A volume of 1 ml leaf extract was treated with a few drops of 5% neutral ferric chloride.

Test for Saponins (Frothing Test): About 1 mL of the leaf extract was diluted separately with 5 mL of distilled water and was shaken in a test tube for 15 min.

Preparation of NiO-NPs

The biosynthesis of the NiO-NPs was carried out according to Ferenji et al. (11) with some modifications. In a 250 mL Erlenmeyer flask, 5 g of $Ni(NO_3)_2 \bullet 6H_2O$ were dissolved in 100 mL of the *citrus limon* leaf extract. The pH was adjusted to 10.0 using a 0.1M NaOH solution and then kept under continuous stirring (900rpm) at 80°C for 4 h. The mixture showed a color alteration from a green precipitate to yellowish-brown gel material, indicating the formation of NiO-NPs. The gel mixture product was then centrifuged at 5,500 rpm for 10 min, and the pellet was washed several times with distilled water and then with ethanol. The pure NiO-NPs were then dried in an oven at 100°C for 10 h. Finally, the dry green powder was calcinated in an oven furnace at 400°C for 2h to form a grayish black powder of NiO-NPs, which was then used for characterization. Figure 1 summarizes the green synthesis, characterization and adsorption studies of the NiO-NPs.

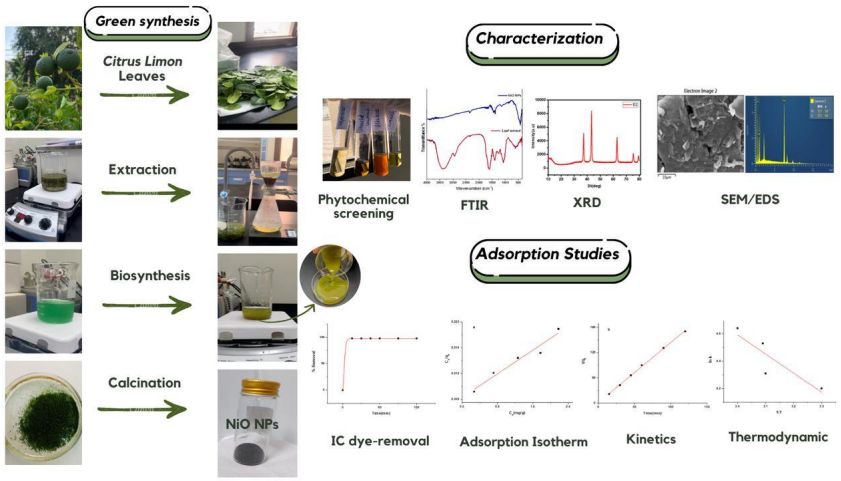

Figure 1: A schematic diagram of the overall green synthesis, characterization and adsorption studies of the biosynthesized NiO-NPs using *citrus limon* leaf extract.

Characterization of NiO-NPs

The NiO-NPs were characterized using an X-ray diffractometer (XRD, Rigaku, Tokyo, Japan, with K beta filter, time duration 10.000°/min, scanning range 10.0–90.0°, and operated at 40 kV, 40 mA), Shimadzu Fourier Transform Infrared Spectrophotometer (FTIR, 4000–400 cm^{-1}, fixed path length, Kyoto, Japan), The elementary calculation was identified using the energy dispersive X-ray spectroscopy (EDS), whereas the surface morphology of the NPs was verified using SEM (FESEM, JEOL-SEM, 6700F, Tokyo, Japan). Surface properties were estimated

using the (BET) model from nitrogen adsorption isotherms collected at 77K using a NOVA 2200e surface area analyzer, Durham, England. Pore size distribution was analyzed using a BJH model from the desorption branch. The thermogravimetric analysis TGA/DSC were carried out using the Perkin Elmer Pyris 1 TGA. The pH measurements were carried out using a pH meter (BOECO, model PT-380, Germany). The IC dye concentration in the sample solutions was determined at λ_{max} at 610.5 nm using a double beam UV-vis. spectrophotometer (UV-3600, Shimadzu, Hamburg, Germany).

Dye Adsorption Studies

The IC dye was chosen to study the dye removal activity and adsorption capacity of NiO-NPs under different adsorption parameters: dye concentration, adsorbent dose, contact time, pH, and temperature. The stock IC solution (100 ppm) was prepared in double-distilled water, and the serial dye concentrations were obtained by the dilution method. In a 250 ml graduated beaker, a known amount of NiO-NPs was added to 100 ml dye solution, and the mixture was allowed to stir at 900 rpm in the dark for 30 min in order to reach equilibrium. The residual concentration of the dye was measured using a UV-vis. spectrophotometer in the range of 400–800 nm. Prior to adsorption experiments, the λ_{max} of the absorption band of the IC solution was determined in the range of 400–800 nm. The different pH of the IC solution was maintained using 0.1 M HCl and 0.1 M NaOH solutions. The ranges of the different adsorption parameters used were as follows: dye concentrations (15–100 ppm), contact time (0–120 min.), adsorbent dose (20–100 mg), pH (3–11), and temperature (30–60 °C). Each experiment was carried out in triplicates, and the dye concentration was determined at λ_{max} 610.5 nm. The adsorption experiments were carried out to measure the adsorption uptake quantity (q_e) and the percentage of dye removal (%R) of IC on the NiO-NPs adsorbent using the following equations.

$$q_e = \frac{C_0 - C_e}{W} x\ V \qquad (1)$$

$$\%\mathrm{R} = \frac{C_o - C_e}{C_0} x\ 100 \qquad (2)$$

where q_e is the equilibrium adsorption capacity (mg/g); C_0 and C_e are the initial and equilibrium concentrations (mg/L) of the adsorbent solution, respectively; V is the volume of the initial solution (L) used for sorption; and W is the weight of the adsorbent (g). The analytical response was expressed as the adsorption efficiency (%R).

3. Results and discussion

Table 1 and figure 2 summarizes the phytochemical screening results of the main bioactive components of the *citrus limon* leaf extract. Positive results were obtained, indicating that *citrus limon* leaf extract possesses the mentioned bioactive compounds. These results are consistent with the findings of J.M. Ehiobu et al. (8), which reported high contents of phenols, flavonoids, saponins, and alkaloids, with the highest phenolic acid and flavonoid content in the aqueous *citrus limon* leaf extract.

Table 1: Phytochemical analysis of the *citrus limon* leaf extract.

s.n.	**Phytochemicals**	**Chemical test**	**Results**
1	flavonoids	alkaline test	+
2	alkaloids	Wagner's test	+
3	Phenolic compounds	Ferric Chloride	+
4	saponins	frothing test	+

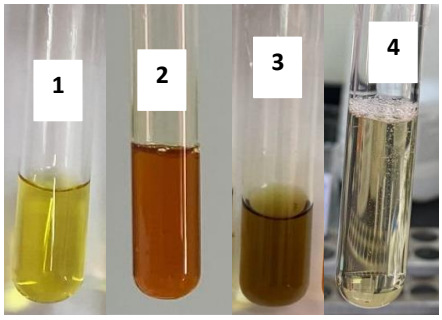

Figure 2: A photographic image of the results of the phytochemical test *citrus limon* leaf extract.

FTIR analysis

Figure 3 shows the FTIR spectra of the *citrus limon* leaf extract and that of the NiO NPs were measured in the range of (4000–400 cm^{-1}). The FTIR spectrum of leaf extract showed two broad bands at 3387 cm^{-1} and 627 cm^{-1}, which could be attributed to the stretching and bending vibrations of the OH group in phenolic compounds, alcohols, and carboxylic acids, respectively. The absorption band at 1624 cm^{-1} indicated the presence of the C=O group, and the peaks in the range 1535–1410 cm^{-1} were attributed to the aromatic C=C bond. The absorption band appeared at 1078 cm^{-1} and was assigned to the C-O stretching frequency. These

results are consistent with the FTIR spectra of phenolic compounds and flavonoids(13). Moreover, this suggests that bioactive compounds present in lemon leaf extract are involved in the bio-reduction and stabilization of nickel ions to nickel oxide nanoparticles (13, 14).

The FTIR spectrum of NiO-NPs (figure 3) showed a strong broad band at 422 cm^{-1} attributed to Ni–O stretching frequency, which confirmed the formation of the NiO-NPs. The absorption band at 1438 cm^{-1} may be ascribed to H–O–H bending vibration of the traces of water molecules adsorbed on the surface of the or to the C=O stretching vibrations (6, 7).

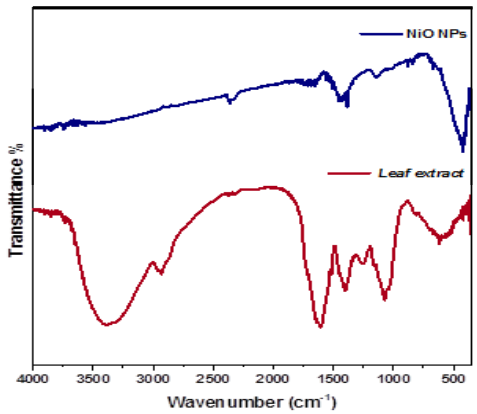

Figure 3: FTIR spectra of *citrus limon* leaf extract and the NiO-NPs.

XRD analysis

The crystal structure of the synthesized NiO-NPs was characterized using the XRD technique. The results showed the presence of five strong diffraction peaks at (2Θ = 37, 43, 63, 75.5, 79.5°) corresponding to Miller Indices (111, 200, 202, 311, 222), respectively. These reflections indicated that the formed nanoparticles have a cubic crystalline structure with the space group Fm-3m (COD 1010095). The XRD examination of the NiO-NPs shown in figure 4 matches the XRD spectrum according to the COD data of NiO (1010095). There were no additional peaks in the XRD spectrum, confirming the purity of the obtained nanoparticles. The particle size of the nanoparticles was estimated using the Debye-Scherrer equation, and the average crystalline size was found to be 14.5 nm (13).

$$D = K\lambda / \beta \cos \theta$$

where D is the average crystal size of the nanomaterial, k is the Scherer coefficient (0.94), λ is the wavelength of X-rays (λ = 0.154 nm), θ is the Bragg angle 2θ, and β is the full width at half maximum (FWHM) in radians.

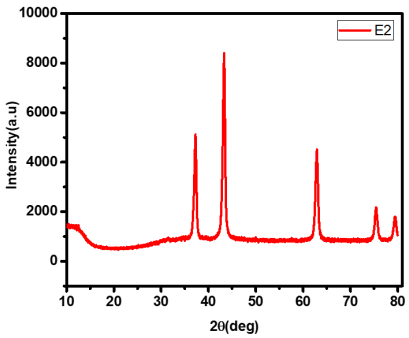

Figure 4: XRD diffraction pattern of the NiO-NPs

SEM/EDS analysis

The morphological features of NiO NPs were examined using SEM analysis (figure 5a). The image showed that the nanoparticles had cubic shape morphology with high agglomeration with an average particle size of 374 nm. The agglomeration of nanoparticles may be due to the exposure of the particles to high calcination temperature (5), or maybe due to aggregation or overlapping of smaller particles, which is in good agreement with results reported in the literature (14, 15). EDS spectrum (figure 5b) reveals the presence and formation of Ni (72.5%) and O (27.5%) in total weight percentage of NiO-NPs. No extra elemental peaks were found, which gives evidence of successful formation of NiO NPs with high purity. The results of the EDS analysis of the NiO-NPs were compatible with the XRD results (11).

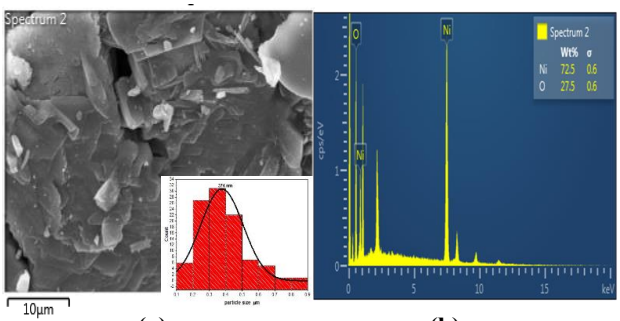

Figure 5: (a) SEM image with insert of particle size distribution curve b) EDS pattern of the NiO-NPs.

BET analysis

The N_2 adsorption/desorption experiment was conducted at 77 K in order to determine the adsorption capacity of the adsorbent material. The BET values calculated from the N_2 adsorption/desorption isotherms for surface area, pore volume, and pore size of NiO-NPs were found to be 13.459 m^2/g, 4.98 nm, and 0.036 cm^3/g, respectively. Figures 6 (a) and (b) show the N_2 desorption isotherms and the pore size distribution curves of the biosynthesized nanomaterial. The resulting hysteresis ring HI obtained from the N_2 adsorption isotherms of the pure NiO-NPs exhibited a type-IV isotherm indicating that the charge surface of the adsorbent is neutral. The pore size (4.9 nm) and the mesoporous structure of the nanomaterial were in good agreement with the IUPAC pore size, confirming the mesoporous classification and properties. The NiO-NPs showed a homogeneous size distribution, a mesoporous structure, and a large specific surface area, indicating a good adsorption capacity towards the desired adsorbates. Consequently, higher percentages of IC dye removal are expected to occur at a shorter contact time (16).

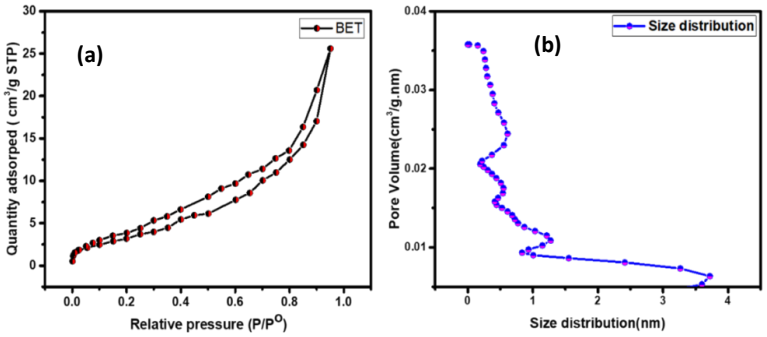

Figure 6: a) N_2 adsorption-desorption isotherm and b) BJH pore-size distribution curve for NiO-NPs sample at 77 K.

TGA analysis

The samples' thermal stability and breakdown properties were examined using TGA. The TG curves are shown in figure 7. A notable rise is seen in the TG data at 299.29°C, which is explained by an exothermic effect connected to the breakdown of epoxy and carboxyl functional groups as well as the evaporation of physically adsorbed water (17). The temperature at which significant weight loss results from the disintegration of these components is indicated by this peak. The weight change observed ranges from 40.80% to 99.99%, reflecting the progressive dehydration and dehydroxylation of present in the samples. This analysis underscores the thermal behavior of the adsorbents, providing insights into their stability and potential applications in adsorption processes under varying thermal conditions. TGA was performed to determine the thermal properties of the NiO-

NPs. The temperature was changed from 37.5°C (room temp.) to 1200°C for a sample of 14.8 mg placed in an aluminum pan at a heating rate of 20°C/min under an air atmosphere. The initial mass loss begins with the peak at 100°C, which is related to the moisture content of the sample, which was calculated and found to be 10%. The two small peaks at 600°C and 800°C correspond to mass loss of 45% and 49%, respectively, and may be related to self-gasification of possibly formed char (18).

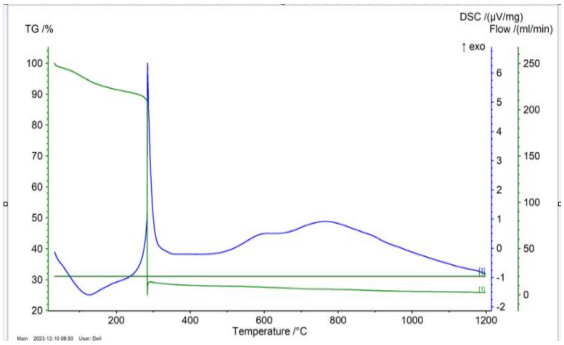

Figure 7: TGA for NiO-NPs surface.

Adsorption Studies

Effect of dye concentration

The effects of the dye's starting concentration (298 K, NiO-NPs dose of 50 mg, 30-min adsorption period, and 150 rpm shaking speed) on the adsorption process were examined using various concentrations the IC dye (15, 30, 45, 60, and mg/L). As the initial concentration of IC dye rises. Figure 8 a,b illustrates that the amount of adsorbed dye (q_e) rises from 29.45 to 145.64 mg/g, but the removal percentage (%R) falls from 98.18% to 97.19%. Once the initial IC dye concentration fills the adsorbent surface sites, saturation is achieved at a lower dye concentration. Therefore, adding more IC dye to a solution does not result in further adsorption; rather, at greater concentrations, it actually reduces dye removal (Figure 8a). Figure 8b illustrates that the amount of adsorbed dye, q_e, increases in tandem with the initial IC dye concentration. This may be because sorption becomes independent of starting concentration at low initial IC values due to the limited number of accessible sites per unit dye concentration. On the other hand, more IC molecules become available per unit mass as dye concentration increases, which causes the binding sites to gradually fill and q_e values to climb (19).

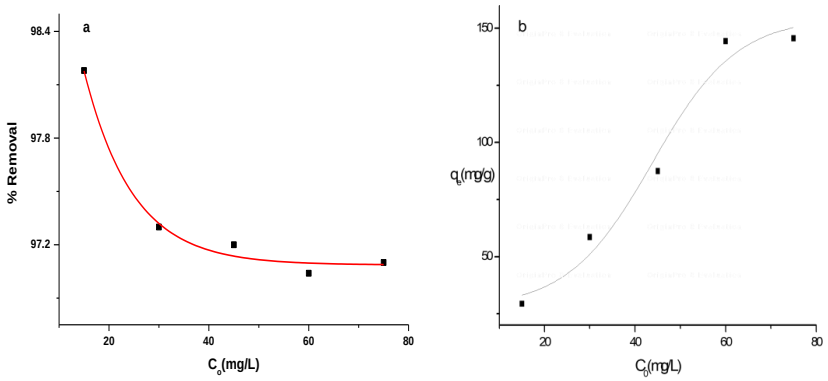

Figure 8: Effect IC dye concentration (a) Removal percentage (%R), (b) Amount of adsorbed dye (q_e)

Effect of NiO-NPs doses

The impact of NiO-NPs weight on the removal percentage of IC dye was examined using adsorbents containing 20, 40, 60, 80 and 100 mg. Additional conditions for the experiment included a 30-min adsorption duration and an initial IC dye concentration of 30 mg/L. Figure 9 illustrates how the weight of NiO-NPs affects the percentage of IC dye elimination. This graph demonstrates that when the weight of NiO-NPs increased, the R% value rose from 96.65% to 97.63%. This rise is correlated with both the adsorbent's surface area and the number of accessible adsorption sites. Based on the obtained results, 100 mg was determined to be the ideal weight for further research (20).

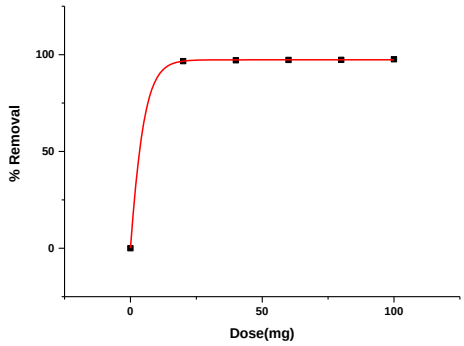

Figure 9: The effect of NiO-NPs weight on the % removal of IC dye.

Effect of adsorption time

By varying the adsorption duration from 15 to 120 min at 298 K and using a 50 mg dosage of NiO-NPs, the effect of adsorption time on the elimination percentage for 50 mg/L IC dye was investigated. The impact of adsorption time on the IC dye elimination percentage is depicted in figure 10. It is evident that the %R number abruptly rises at 15 min and then nearly stabilizes at 45 min. This may be explained by the presence of vacant adsorption sites on the surfaces of NiO-NPs, which were then slightly increased until the equilibrium was attained. Thus, 60 min was the ideal duration (21).

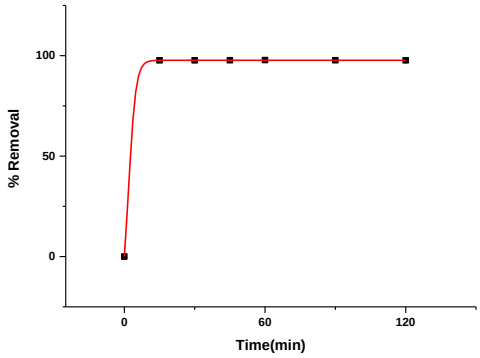

Figure 10: The effect of adsorption time on the % removal of IC dye.

Effect of temperature

Under ideal operating conditions, which included an initial IC dye concentration of 30 mg/L, a NiO-NPs dose of 50 mg, an adsorption period of 30 min, and a temperature variation from 303 to 333 K, the impact of temperature on the percentage removal of IC dye was examined. Figure 11, which displays the results, shows that the percentage removal (R%) grows with temperature. This implies that the sorption process may be responsible for the exothermic IC dye adsorption onto NiO-NPs (22).

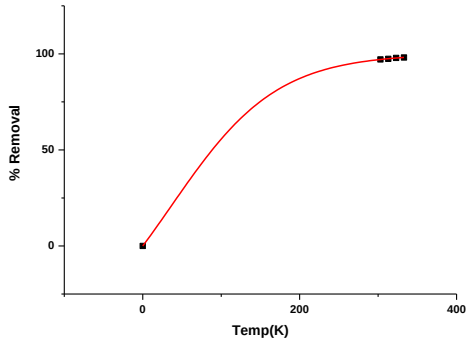

Figure 11: The effect of temperature on % removal of IC dye

Effect of initial pH

By varying the pH between 3 and 11 at 298 K, with an IC dye concentration of 30 mg/L, an adsorbent dosage of 50 mg, and an adsorption period of 30 min, the impact of pH on the % R was examined. Figure 12 illustrates how pH affects the proportion of IC dye removed using NiO-NPs. The figure shows that when the pH values increased, the %R values dropped from 98.18% to 84.5%. Since the adsorbent surface has a high positive charge density at lower pH values, the adsorption of the anionic dye can be enhanced in acidic environments. Higher values for removal will therefore be established as a result of the electrostatic attraction between the positively charged surface and the negatively charged IC dye, whereas at higher pH values, there is an increase in the negatively charged sites associated with the presence of OH ions, which results in electrostatic repulsion, as observed (23).

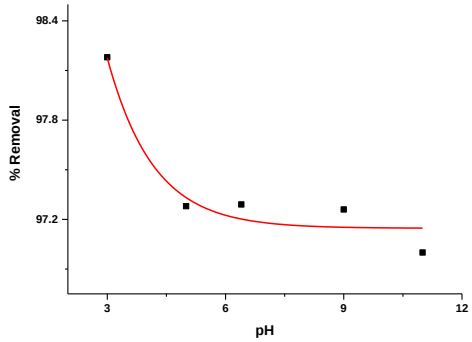

Figure 12: The effect of pH solution on the % removal IC dye.

Adsorption isotherm models

Langmuir isotherm

This model states that there is no interaction between molecules adsorbing on different locations and that the adsorption surface layer is uniform with identical spots for all adsorbate molecules. A signal adsorbate molecule is also thought to be able to occupy an active site, resulting in a single molecule as the thickness of the adsorption layer. The following equation represents this model's linear equation:

$$\frac{C_e}{q_e} = \frac{1}{q_{max}.b} + \frac{1}{q_{max}} .Ce \qquad (3)$$

Where Ce is the dye concentration at equilibrium (mg/L), q_e refers to the equilibrium amount of the substance adsorbed per gram of the adsorbent (mg/g), q_{max} is the maximum monolayer coverage (mg/g), and b is the Langmuir isotherm constant (L/mg). The values of b and q_{max} are estimated from the linear plot between C_e/q_e against C_e (figure 13a). The effectiveness of adsorption was calculated using the dimensionless constant or separation factor R_L which was estimated using the following equation.

$$R_L = \frac{1}{b_{Ci}} \qquad (4)$$

Where C_i is the starting IC dye concentration (mg L^{-1}). The values of Rs specifies the adsorption was irreversible R = 0, favorable (0 < R_L < 1), linear R_L = 1 or unfavorable R_L >1. The values of b, q_{max} and R_L are listed in Table 2. From the values of R_L it can be noticed that these values between 0 and 1 (0 < R_L < 1) which indicates that the adsorption of IC dye onto NiO-NPs favorable.

Freundlich isotherm

The Freundlich linear equation can be written as following equation (24):

$$\log q_e = \log K_f + \frac{1}{n} \log C_e \qquad (5)$$

Where k_f is Freundlich constant related to the adsorption capacity (mg/g) and n_f is the adsorption intensity, these values were estimated from the intercept and slope of linear relation between ln q_e and ln C_e (figure 13b). Table 2 displays the values that were obtained. The sorption of IC dye onto NiO-NPs is advantageous, as can be observed from the values of $1/n_f$ < 1. It may be inferred from the correlation coefficient R^2 values for both models that Langmuir models well represent the experimental data. Our findings concur with N. H. Al-Shammari et al (25). Adsorption is thought to benefit from n values between 1 and 10, with n > 1 being

the most prevalent and explaining the distribution of active centers on the surface or any other factor that causes the adsorbent-adsorbate interaction to diminish as surface density increases. A physical adsorption of IC ions onto the NiO-NPs is indicated if n is between 1 and 10 (1/n is smaller than 1). Table 3 compares the results of this study to those of the previous findings.

Table 2: Adsorption isotherm models' constants.

Isotherm model	R_L	Evaluated parameters of the isotherm		
Langmuir	0.06	q_{max} (mg/g)	b (L/mg)	R^2
		218	0.54	0.95
Freundlich	-	n	K_f	R^2
	-	2.5	4.51	0.98

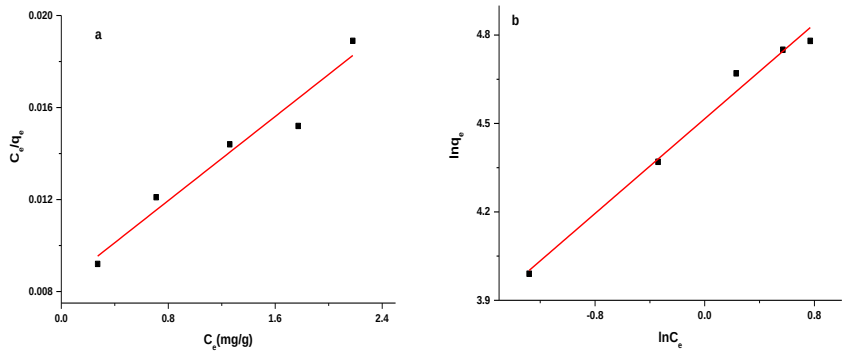

Figure 13: Adsorption isotherm plots for (a) Langmuir isotherm (b) Freundlich isotherm.

Table 3: A Comparison of the maximum monolayer adsorption of some dyes on various adsorbents.

Dye	Adsorbent	Maximum monolayer adsorption capacity (mg g^{-1})	References
Methylene Blue (MB)	Orange peels	98.9	(26)
Methylene Blue (MB)	Nano activated carbon	28.09	(27)
Methyl orange (MO)	(NiO-NPs)	97.56	(6)
Indigo Carmine (IC)	(NiO-NPs)	218.4	our study

Adsorption Kinetics model

The pseudo-first order PFO (Lagergren equation) written as following:

$$\ln(q_e - q_t) = \ln q_e - k_1 . t \qquad (6)$$

Where q_t, q_e are the amount adsorbed at time t and at equilibrium (mg. g^{-1}), respectively, For the adsorption process, t is the time (min), and k_1 is the PFO rate constant (min^{-1}). PFO rate constants k_1 and qe were estimated using the slopes and intercepts of the plots between ln (q_e-q_t) against t in figure 14a. Table 4 provided a summary of these values. The lack of fitting agreement between the values of q_e cal and q_e exp is evident from the data, indicating that this model is less appropriate for explaining the adsorption process. The following is the expression for the pseudo-second order (PSO) kinetics equation:

$$\frac{t}{q_t} = \frac{1}{k_2 q_e^2} + \frac{1}{q_e} . t \qquad (7)$$

Where k_2 is the equilibrium rate constant for the PSO equation (g/mg. min). The values of k_2 and q_e can be estimated from the intercept and the slope of plots between t/qt versus t as shown in figure 14b, these values are shown in Table 4. According to the obtained results, it is clear that the values of correlation coefficients R^2 for the PSO model was higher than PFO model, also there is a good agreement between the values of q_e exp and q_e cal, so we can suggest that the PSO sorption mechanism is predominant.

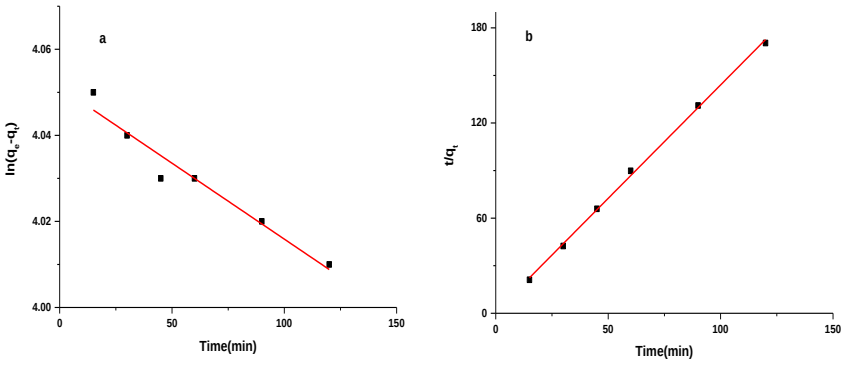

Figure 14: Adsorption kinetic plots for (a) PFO model (b) PSO model.

Table 4: Kinetic parameters and correlation coefficients for IC adsorption on NiO-NPs.

Pseudo-first order		**Pseudo-second order**		**Experimental q_e**
q_e,cal (mg/g)	177.08	q_e,cal (mg/g)	208 (mg/g)	218 (mg/g)
K_1 (min^{-1})	-3.52	K_2 (min^{-1})	0.005	
R^2	0.99	R^2	0.95	

Adsorption Thermodynamics

Thermodynamic parameters values are calculated using the following equations:

$$lnK_{ads} = \frac{\Delta S}{R} - \frac{\Delta H}{RT} \quad (8)$$

$$\Delta G = -RTlnK \quad (9)$$

where ΔS° represents the change in entropy with unit J/mol K and ΔH° shows the variation in enthalpy with unit kJ/mol. The slope and intercept of the plot between the values of ln Kq_e against 1/T (figure 15) yield the values of ΔH° and ΔS°. Table 5 reports on the values. Negative values for the change in the Gibbs free energy ΔG° at the specified temperature were used to assume that the adsorption process was spontaneous; however, negative values for ΔH° indicated that the process was exothermic. This could be explained by the sorption process, which combines absorption and adsorption. Furthermore, when IC dye is adsorbed onto NiO-NPs, the positive ΔS° values show that the degrees of randomness are almost increased at the solid-liquid interface (28).

Table 5: Thermodynamic parameters for IC adsorption on NiO-NPs.

T (K)	**ΔG° (J/mol)**	**ΔH° (J/mol)**	**ΔS° (J/mol.k)**
30	-105.8	-11.51	72.98
40	-112.1		
50	-121.6		
60	-128.46		

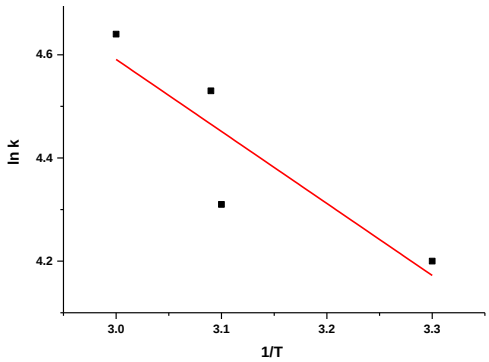

Figure 15: Thermodynamics adsorption of IC dye onto NiO-NPs.

4 Conclusions

A simple, clean, green approach has been established for the synthesis of NiO-NPs using *citrus limon* leaf extract as a reducing and stabilizing agent. The FTIR, XRD and EDS analyses confirmed the formation of pure, crystalline nature and the elemental composition of the biosynthesized NiO-NPs. The XRD pattern indicated a cubic crystalline phase with crystallite size of 14.5 nm which could be attributed the action of different phytochemicals present in the leaf extract. The NiO-NPs synthesis and its characterization of chemically stable spheres highlight their advantages toward the environment. The outcomes indicate that NiO-NPs give rapid adsorption, to reach equilibrium within approximately 30 min and the removal efficiencies for IC dye were notably high with values of 96 %, 97 %, 98.25 %, and 99.82 % at equilibrium. The adsorption of IC onto the NiO-NPs sample was well-fitted by the Langmuir isotherm model. It was discovered that the adsorption process is exothermic and happens spontaneously based on the thermodynamic parameters ΔH^o, ΔS^o, and ΔG^o. The best model for describing the adsorption kinetics, according to the kinetics study's findings, was pseudo second order prospective. Herein, the findings were found to be compatible with the resent researches reported in literature (22, 29, 30). This work sets the stage for further investigation into how to best utilize and scale up the application of NiO-NPs for the efficient removal of IC dye under varied environmental circumstances, thereby fostering more robust ecosystems and protecting human health.

Acknowledgments: The authors are grateful for the technical support of the Chemistry Department at the College of Science, Qassim University.

Conflicts of Interest: The authors declare no conflicts of interest.

References

.1 El-Kammah M, Elkhatib E, Gouveia S, Cameselle C, Aboukila E. Cost-effective ecofriendly nanoparticles for rapid and efficient indigo carmine dye removal from wastewater: Adsorption equilibrium, kinetics and mechanism. Environmental Technology & Innovation. 2022;28:102595.
.2 Nnadozie EC, Ajibade PA. Isotherm, kinetics, thermodynamics studies and effects of carbonization temperature on adsorption of Indigo Carmine (IC) dye using C. odorata biochar. Chemical Data Collections. 2021;33:100673.
.3 Nasrollahzadeh M, Sajjadi M, Iravani S, Varma RS. Green-synthesized nanocatalysts and nanomaterials for water treatment: Current challenges and future perspectives. Journal of hazardous materials. 2021;401:123401.
.4 Verma R, Chauhan MS, Pandey S, Dandia A. Reduced graphene Oxide/NiO based nano-composites for the efficient removal of alizarin dye, indigo dye and reduction of nitro aromatic compounds. Heliyon. 2023;9.(6)
.5 Rashid IM, Salman SD, Mohammed AK, Mahdi YS. Green synthesis of nickle oxide nanoparticles for adsorption of dyes. Sains Malaysiana. 2022;51(2):533-46.
.6 Riaz Q, Ahmed M, Zafar MN, Zubair M, Nazar MF, Sumrra SH, et al. NiO nanoparticles for enhanced removal of methyl orange: equilibrium, kinetics, thermodynamic and desorption studies. International Journal of Environmental Analytical Chemistry. 2022;102(1):84-103.
.7 Athab ZH, Halbus AF, Mohammed SB, Atiyah AJ, Ismael HI, Saddam NS, et al. Comparison activity of pure and chromium-doped nickel oxide nanoparticles for the selective removal of dyes from water. Scientific Reports. 2024;14(1):4032.
.8 Ehiobu J, Idamokoro M, Afolayan A. Phytochemical content and antioxidant potential of leaf extracts of Citrus limon (L.) Osbeck collected in the Eastern Cape Province, South Africa. South African Journal of Botany. 2021;141:480-6.
.9 Thapa S, Poudel K, Limbu SK, Dahal G, Pokhrel S. Phytochemical screening, GC analysis and antibacterial activity of Citrus limon peel extract and essential oil. Journal of Nepal Chemical Society. 2022;43(1):69-75.
.10 Gupta S, Rahman MA, Sundaram S. Citrus fruit as A potential source of phytochemical, antioxidant and pharmacological ingredients. JSHE. 2021;2581:8473.
.11 Ferenji AE, Hassen YE, Mekuria SL, Girma WM. Biogenic mediated green synthesis of NiO nanoparticles for adsorptive removal of lead from aqueous solution. Heliyon. 2024;10.(11)
.12 Hooda R, Sharma M. Green synthesis, characterization and antibacterial activity of iron oxide nanoparticles. 2020.
.13 Alharbi FN, Abaker ZM, Makawi SZA. Phytochemical substances—mediated synthesis of zinc oxide nanoparticles (ZnO NPS). Inorganics. 2023;11(8):328.
.14 Firisa SG, Muleta GG, Yimer AA. Synthesis of nickel oxide nanoparticles and copper-doped nickel oxide nanocomposites using phytolacca dodecandra

l'herit leaf extract and evaluation of its antioxidant and photocatalytic activities. ACS omega. 2022;7(49):44720-32.
.15 Pooyandeh S, Shahidi S, Khajehnezhad A, Ghoranneviss Z. Synthesizing and deposition of nickel oxide nanoparticles on glass mat using sol–gel method (morphological and magnetic properties). The Journal of The Textile Institute. 2021;112(6):887-95.
.16 Rafat A, Hashemian S, Shishabor MR. Preparation and characterization of nano composites from metal oxides and activated carbon from banana peel (MO@ BPAC, MO= NiO, CuO and ZnO) for 2 nitrophenol removal from aqueous solutions. Heliyon. 2025;11(1.(
.17 Pouangam Ngalani G, Ondo JA, Njimou JR, Nanseu Njiki CP, Prudent P, Ngameni E. Effect of coffee husk and cocoa pods biochar on phosphorus fixation and release processes in acid soils from West Cameroon. Soil Use and Management. 2023;39(2):817-32.
.18 Müller L, Rubio-Pérez G, Bach A, Muñoz-Rujas N, Aguilar F, Worlitschek J. Consistent DSC and TGA methodology as basis for the measurement and comparison of thermo-physical properties of phase change materials. Materials. 2020;13(20):4486.
.19 Ramutshatsha-Makhwedzha D, Mavhungu A, Moropeng ML, Mbaya R. Activated carbon derived from waste orange and lemon peels for the adsorption of methyl orange and methylene blue dyes from wastewater. Heliyon. 2022;8.(8)
.20 Al-Qadri FA, Alsaiari R. Silica ash from waste palm fronds used as an eco-friendly, sustainable adsorbent for the Removal of cupper (II). Archives of Environmental Protection. 2023;49.(2)
.21 Alkorbi F, A Al-Qadri F. Peganum Harmala seeds extract: A green synthesis route for Mn-doped ZnO nanoparticles as an adsorbent for crystal violet dye removal. Archives of Environmental Protection. 2024:43-53-43-53.
.22 Raman G, Kumar US, Vasumathi V, Muthu K. Improving photocatalytic performance of nickel oxide infused chitosan nanocomposite for adsorption of organic dyes. Surfaces and Interfaces. 2025;56:105505.
.23 Ali OS, AL-Mammar DE. Adsorption of the Color Pollutant onto NiO Nanoparticles Prepared by a New Green Method. Iraqi Journal of Science. 2024:1824-38.
.24 Vitek R, Masini JC. Nonlinear regression for treating adsorption isotherm data to characterize new sorbents: Advantages over linearization demonstrated with simulated and experimental data. Heliyon. 2023;9.(4)
.25 AL-Shammari NH, AL-Mammar DE. Adsorption of Biebrich Scarlet Dye into Remains Chromium and Vegetable Tanned Leather as Adsorbents. Iraqi Journal of Science. 2022:2814-26.
.26 Gunay Gurer A, Aktas K, Ozkaleli Akcetin M, Erdem Unsar A, Asilturk M. Adsorption isotherms, thermodynamics, and kinetic modeling of methylene

blue onto novel carbonaceous adsorbent derived from bitter orange peels. Water, Air, & Soil Pollution. 2021;232:1-17.

.27 Shokry MM, Sadek MF, Osman AF, El Kalioubi BA. Precambrian basement rocks of Wadi-Khuda-Shut area, South Eastern Desert of Egypt: Geology and remote sensing analysis. The Egyptian Journal of Remote Sensing and Space Science. 2021;24(1):59-75.

.28 Kadhim HH, Saleh KA. Removing cobalt ions from industrial wastewater using chitosan. Iraqi Journal of Science. 2022:3251-63.

.29 Khalid R, Raza S, Areej I, Ashraf F, Abid A. Green Synthesis of Nickel Oxide Nano particles from Lawasonia inermis leaf extract for promising Methyl red Uptake and Efficient Iodine Adsorption. 202.4

.30 Agalya S, Nehru L, Sagadevan S. Green-synthesized nickel oxide nanoparticles for sustainable wastewater treatment and enhanced bacterial control. Ceramics International. 2024;50(23):50185-9